AAPT PHYSICS EDUCATION | AMERICAN JOURNAL of PHYSICS

The Kronig-Penney model extended to arbitrary potentials via numerical matrix mechanics

R. L. Pavelich and F. Marsiglio

Citation: American Journal of Physics **83**, 773 (2015); doi: 10.1119/1.4923026
View online: http://dx.doi.org/10.1119/1.4923026
View Table of Contents: http://scitation.aip.org/content/aapt/journal/ajp/83/9?ver=pdfcov
Published by the American Association of Physics Teachers

The Kronig-Penney model extended to arbitrary potentials via numerical matrix mechanics

R. L. Pavelich[a] and F. Marsiglio[b]
Department of Physics, University of Alberta, Edmonton, Alberta, Canada T6G 2E1

(Received 16 September 2014; accepted 11 June 2015)

The Kronig-Penney model is a common starting point for studying the quantum mechanics of electrons in a confining periodic potential. This model uses a square-well potential; the energies and eigenstates can be obtained analytically for a single well, and then Bloch's theorem allows one to extend these solutions to the periodically repeating potential. In this work, we describe how to obtain simple numerical solutions for the eigenvalues and eigenstates for any confining one-dimensional potential within a unit cell and then extend this procedure, with virtually no extra effort, to the case of arbitrary periodically repeating potentials. In this way, one can study the band structure effects that arise from differently shaped potentials. One of these effects is the electron-hole mass asymmetry; more realistic unit cell potentials generally give rise to higher electron-hole mass asymmetries. © *2015 American Association of Physics Teachers.*
[http://dx.doi.org/10.1119/1.4923026]

I. INTRODUCTION

The Kronig-Penney model[1] remains the paradigm for the demonstration of energy bands, separated by gaps, in periodic solids. The concept of energy bands in turn is used to introduce the notion of metals vs (band) insulators, based on the level of the chemical potential (and therefore dependent on the number of electrons) in the solid. The model is appealing insofar as it only requires solutions to the Schrödinger equation for the simplest potential (a constant) and the equation for determining the allowed energies can be written analytically in terms of elementary functions. This exercise is also enlightening as it offers a clear application of Bloch's theorem,[2] which can seem fairly abstract when first introduced, and it also illustrates how boundary conditions are paramount in determining the energy spectrum. The energies themselves are readily determined through an explicit equation, and can be easily obtained with a calculator. Even more important, perhaps, is that in one particular limit of the model, the so-called Dirac comb, where the barriers become infinitely thin while their heights become infinitely high (i.e., a periodic series of δ-functions), the existence of energy gaps can be demonstrated analytically.

All of these features are beneficial and even desirable for pedagogical reasons, but often one would like to demonstrate the same ideas for more complicated (and realistic) potentials. In other words, it naturally occurs to students at some point to inquire about the generality of the conclusions reached through an idealized model. Furthermore, for graduate students there tends to be a quantum leap from the analytical solution of the Kronig-Penney model to the numerical (black-box-like) methods used in realistic electronic band structure calculations.[3] In this paper, we propose to bridge this gap somewhat with simple, albeit numerical, solutions for an arbitrary unit-cell potential, still in one dimension.

The basic idea comes from some recent work concerning simple one-body potentials.[4,5] We will describe this work in Sec. II and follow it with the alterations necessary to utilize periodic (as opposed to open) boundary conditions. This change allows us to proceed and replace the periodic boundary condition with the Bloch condition. We can then compare our numerically derived results with the known analytic ones, to establish the validity and accuracy of the method. Note that an alternate procedure would be to simply define a periodic potential that repeats a finite number of times, say ten or twelve, and solve the Schrödinger equation for this potential. This was done, for example, in Ref. 6, by solving the differential equation using a "hunt and shoot" method. Here, we prefer to use the matrix diagonalization method,[4] and we prefer to incorporate Bloch's theorem analytically, for the sake of efficiency and pedagogy. Furthermore, in the present approach, there are no finite-size effects, and the wave vector is a continuous variable. In Sec. IV, we explore a number of fairly different unit-cell potentials; freedom to choose the parameters that characterize these potentials allows each to have various bandwidths and effective masses. One particular feature that is shape-dependent is the asymmetry in electron/hole effective mass. We summarize our results in Sec. V and provide a code sample in an Appendix.

II. FORMALISM

A. Infinite square well

By embedding a potential in the infinite square well, one is able to study the bound states of that potential with minimal technical overhead. One has to have access to a numerical matrix diagonalization routine; otherwise only a freshman knowledge of integral calculus and linear algebra is required. The methodology is outlined in Ref. 4, so only key points will be recalled here.

One first expands the wave function in the infinite well basis:

$$|\psi^{(0)}\rangle = \sum_{m=1}^{\infty} c_m |\psi_m^{(0)}\rangle, \tag{1}$$

where the basis states are

$$\psi_n^{(0)}(x) = \begin{cases} \sqrt{\frac{2}{a}} \sin\left(\frac{n\pi}{a}x\right) & 0 < x < a, \\ 0 & \text{otherwise}, \end{cases} \tag{2}$$

with eigenvalues

$$E_n^{(0)} = \frac{n^2\pi^2\hbar^2}{2m_0a^2} \equiv n^2E_1^{(0)}. \tag{3}$$

Here a is the width of the well, and the (unknown) expansion coefficients are c_n. Straightforward algebra leads to the matrix diagonalization problem

$$\sum_{m=1}^{\infty} H_{nm}c_m = Ec_n, \tag{4}$$

where

$$H_{nm} = \langle\psi_n^{(0)}|(H_0+V)|\psi_m^{(0)}\rangle = \delta_{nm}E_n^{(0)} + H_{nm}^V \tag{5}$$

and

$$H_{nm}^V = \langle\psi_n^{(0)}|V|\psi_m^{(0)}\rangle = \frac{2}{a}\int_0^a \mathrm{d}x \sin\left(\frac{n\pi x}{a}\right)V(x)\sin\left(\frac{m\pi x}{a}\right). \tag{6}$$

The problem is easily rendered into a convenient dimensionless form by using units of the infinite square well width a and ground state energy $E_1^{(0)}$

$$\sum_{m=1}^{\infty} h_{nm}c_m = ec_n, \tag{7}$$

where $h_{nm} \equiv H_{nm}/E_1^{(0)}$ and $e \equiv E/E_1^{(0)}$.

B. Square well with periodic boundary conditions

In this work, as a first step, we use the same strategy but instead of a box with infinite walls we use a "box" with periodic boundary conditions. Then the wave function satisfies the general periodicity condition

$$\phi(x+a) = \phi(x), \tag{8}$$

whose solutions are the plane-wave states,

$$\phi(x) \sim e^{ikx}, \tag{9}$$

where $k^2 \equiv 2m_0E/\hbar^2$. Here, k can be either negative or positive. Imposition of the periodicity condition in Eq. (8) then requires

$$ka = 2n\pi, \tag{10}$$

where n is an integer: $n = \ldots -2, -1, 0, 1, 2, \ldots$. The eigenvalues are then

$$E_n = 4\left(\frac{n^2\pi^2\hbar^2}{2m_0a^2}\right) = 4n^2E_1^{(0)}. \tag{11}$$

Note that these differ from the eigenvalues of an infinite square well: (i) they have values that are four times as large for the same integer n; (ii) they are doubly degenerate (with one exception); and (iii) $E=0$ is possible, and also constitutes the one exception to point (ii). The orthonormal basis states are then

$$\phi_n^{(0)}(x) = \sqrt{\frac{1}{a}}\exp\left[i\frac{2\pi n}{a}x\right], \tag{12}$$

where n is an integer.

III. HARMONIC OSCILLATOR

The first question one should ask is, does this basis work? And if so, is this basis any better or worse than the infinite square well basis? To answer these questions we recall the results obtained in Ref. 4 for a harmonic oscillator potential embedded in the infinite square well.

A. Infinite square well basis

We place the harmonic oscillator potential inside an infinite square well of width a that spans $0<x<a$. The analytical form for this potential is

$$V_{\mathrm{HO}}(x) = \frac{1}{2}m_0\omega^2\left(x-\frac{a}{2}\right)^2 \qquad \text{for} \quad 0<x<a, \tag{13}$$

and in dimensionless form we have

$$v_{\mathrm{HO}}(x) = \frac{V_{\mathrm{HO}}(x)}{E_1^{(0)}} = \frac{\pi^2}{4}\left(\frac{\hbar\omega}{E_1^{(0)}}\right)^2\left(\frac{x}{a}-\frac{1}{2}\right)^2 = \left(\frac{\pi\gamma}{2}\right)^2\left(\frac{x}{a}-\frac{1}{2}\right)^2, \tag{14}$$

where we define $\gamma \equiv \hbar\omega/E_1^{(0)}$. Using this potential, the dimensionless Hamiltonian matrix components in the basis (2) are

$$h_{nm} = \frac{H_{nm}}{E_1^{(0)}} = \delta_{nm}\left\{n^2 + \frac{\pi^2\gamma^2}{48}\left[1-\frac{6}{(\pi n)^2}\right]\right\} + (1-\delta_{nm})\gamma^2 g_{mn}, \tag{15}$$

where

$$g_{mn} = \frac{(-1)^{n+m}+1}{4}\left[\frac{1}{(n-m)^2} - \frac{1}{(n+m)^2}\right]. \tag{16}$$

A complete assessment of the success of this approach was carried out in Ref. 4; here we focus on the ground-state wave function to compare with the results from the next subsection. A diagonalization of this matrix with a truncated basis indeed converges to the correct ground-state wave function, and the coefficients in Eq. (1) agree to high accuracy with those expected from the exact analytical solution[7]

$$c_n = \begin{cases} i^{(n-1)}\left(\frac{32}{\pi\gamma}\right)^{1/4}\exp\left(-n^2/\gamma\right) & \text{for } n \text{ odd}, \\ 0 & \text{for } n \text{ even}, \end{cases} \tag{17}$$

where $n = 1, 2, 3, 4, \ldots$. As mentioned in Ref. 4, the excellent convergence for all eigenvalues and eigenvectors can be understood from the $\sim\exp\left(-n^2/\gamma\right)$ dependence expected for

the coefficients for all eigenvectors (not just the ground state), provided that the parameter γ is sufficiently large. This occurs when the well is very wide, so that eigenstates are sufficiently bound by the harmonic potential that they do not even "feel" the infinite walls of the infinite square well. One question that might arise aside from other practical considerations is: can this convergence be improved by adopting different boundary conditions, for example, periodic boundary conditions? The answer to this question is addressed in the next subsection (III B).

B. Periodic boundary conditions

For the case of periodic boundary conditions, we use Eq. (13) but now with the basis states in Eq. (12), so that the matrix elements are

$$H^V_{nm} = \langle \phi^{(0)}_n | V | \phi^{(0)}_m \rangle = \frac{1}{a}\int_0^a \mathrm{d}x\, e^{-i2\pi nx/a}\left[\frac{1}{2}m_0\omega^2\left(x-\frac{a}{2}\right)^2\right]e^{i2\pi mx/a}. \tag{18}$$

This integral is straightforward (some details are given in Appendix A); when combined with the kinetic energy contribution, one obtains

$$h_{nm} = \delta_{nm}\left[4n^2 + \frac{\pi^2\gamma^2}{48}\right] + (1-\delta_{nm})\left[\frac{\gamma^2}{8}\frac{1}{(m-n)^2}\right], \tag{19}$$

which is clearly different from Eq. (15).

As in the infinite-square-well case, we will have to truncate this matrix, so it makes sense to arrange the basis states in order of increasing energy. We will order the quantum numbers as $n = \{0, 1, -1, 2, -2, 3, -3, \ldots\}$, and then truncate at some $n_{\max}$. We will also label the quantum numbers with a new subscript n', where $n' = \{0, 1, 2, 3, 4, 5, 6, \ldots\}$ in the same order. So, for example, $n' = 4$ corresponds to $n = -2$.

In anticipation of our numerical results, it is helpful to calculate the Fourier coefficients of the harmonic oscillator ground state analytically. Using the analytical form for the ground-state wave function written in the same dimensionless units as above,

$$\psi_{\mathrm{HO}}(x) = \left(\frac{\pi\gamma}{2a^2}\right)^{1/4}\exp\left[-\frac{\pi^2\gamma}{4a^2}\left(x-\frac{1}{2}\right)^2\right], \tag{20}$$

we can take the inner product with each eigenstate from Eq. (12). We obtain the coefficients

$$c_{n'} = \langle \phi^{(0)}_n | \psi_{\mathrm{HO}} \rangle = (-1)^n\left(\frac{8}{\pi\gamma}\right)^{1/4}\exp\left(-4n^2/\gamma\right), \tag{21}$$

which again differ from those in Eq. (17). This difference is not significant and shows that no real advantage for convergence can be gained by going to periodic boundary conditions. More importantly, no disadvantage occurs either, as we will illustrate explicitly in the next subsection. Note that the coefficients are labeled by n', but the exponential is calculated with just n, using the correspondence described above.

C. Numerical comparison of periodic and square well basis sets

We pause for a moment to compare the accuracy and efficiency of the two basis sets. In Fig. 1, we plot the numerical eigenenergies obtained for the two cases with $\gamma = 20$ and $n_{\max} = 60$. We use MATLAB's `eig` function,[8] which determines the eigenvalues/vectors by putting the matrix in so-called Hessenberg form and then applying a QR decomposition recurrence scheme that coverges to a so-called Schur decomposition form from which the final values are readily attainable.[9,10] The two basis sets give very similar results, so an expansion in periodic boundary condition basis states is just as effective as the method used in Ref. 4. In particular, either method reproduces the expected linear-in-n results to high accuracy for low-lying states, where the presence of the enclosing box is not even noticed. This is the regime that is physically relevant to the harmonic oscillator potential. At higher values of n both cases produce energies that grow as n^2.

To evaluate the efficiency, we show the results for the coefficients on a semi-log plot in Fig. 2. Both methods yield similar results,[11] with the smooth decay breaking down where $n \approx \hbar\omega/E_1^{(0)}$, which is the condition for the basis state energy equal to the crossover (from harmonic oscillator to square well) energy for the potential. Exact analytical results agree to seven digits in either case. Note that agreement can be systematically improved indefinitely in both cases by enlarging the width of the embedding square well. In practice, this is achieved by increasing the value of γ (note the definition of γ immediately following Eq. (14), where it is clear that $\gamma \propto a^2$). In any event this comparison for the ground state extends to other excited states and shows that neither efficiency nor accuracy is compromised by adopting periodic boundary conditions.

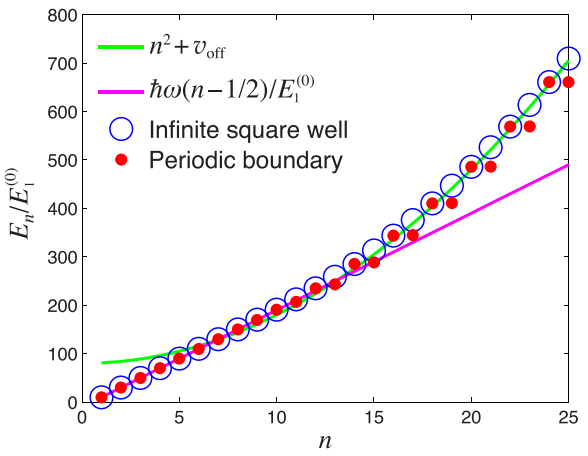

Fig. 1. Plot of the normalized energy levels vs quantum number n for numerical solutions using open (infinite square well) and periodic boundary conditions. We used $n_{\max} = 60$ and $\gamma = \hbar\omega/E_1^{(0)} = 20$. The rationale for the curve $n^2 + v_{\mathrm{off}}$ is explained in Ref. 4. As in Ref. 4, we use an enumeration that starts with $n = 1$ rather than $n = 0$ to make the two cases consistent. Both results give the correct energy eigenvalues at low values of n, and both grow as n^2 at large values of n, reflecting the expected behavior due to the confining box. Note the clear degeneracies at large n for the case with periodic boundary condition energies.

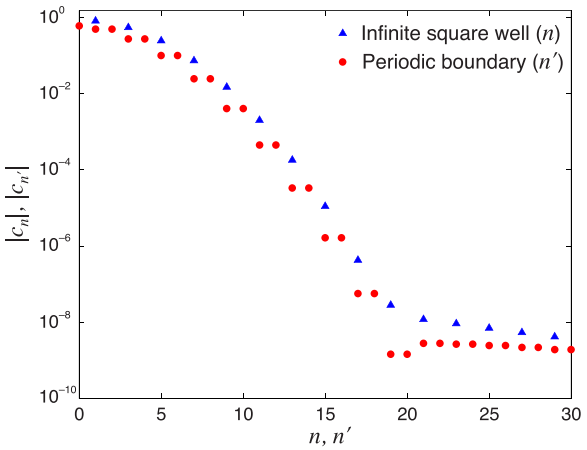

Fig. 2. The numerically derived absolute values of the Fourier coefficients for the infinite square well and the periodic-boundary-condition embedding potentials, plotted on a semi-log graph. The even cases for the infinite square well have finite nonzero results on the order of less than 10^{-15} and are not shown. Here, the truncated matrix dimension is $n_{\max}=60$ and $\gamma=\hbar\omega/E_1^{(0)}=20$. Analytical results cannot be distinguished from the numerical results. We see again that there is little computational difference between the periodic boundary conditions used in this paper and the method used in Ref. 4.

IV. PERIODIC POTENTIALS

A. Bloch's theorem

Bloch's theorem[2] states that the electronic wave function in a periodic potential can be written as a product of a plane wave and a function that has the same periodicity as the potential. Alternatively, one can write

$$\psi(x+a)=e^{iKa}\psi(x), \tag{22}$$

where a is the unit-cell length and K is a wave vector such that $-\pi<Ka<\pi$. Here K is a new quantum number that labels the solutions in each energy band. (In this formalism K is continuous because we have assumed potentials that repeat indefinitely. For a finite-length potential there would be as many solutions in each band as there are cells in the lattice.) Thus, Bloch's theorem allows us to solve for the problem in one unit cell only and allows us to vary K continuously.

B. Analytical solution to the Kronig-Penney model

In practice, the analytical treatment of the Kronig-Penney model[1] allows one to utilize Bloch's theorem as a boundary condition. In that problem, one uses a potential that repeats a square well of width b followed by a square barrier of width $a-b$:

$$V(x)=V_0\sum_{n=-\infty}^{+\infty}\theta[x-(na+b)]\,\theta[(n+1)a-x], \tag{23}$$

where $\theta[x]$ is the Heaviside step function. Note that the width of the unit cell is a and that the product of two θ functions equals 1 within the barrier, where x is greater than $na+b$ but less than $(n+1)a$.

For states whose energies are below the barrier height one can solve the Schrödinger equation for each region in turn: a linear combination of two plane waves in the "well" regions followed by a linear combination of an exponentially decaying and an exponentially growing solution in the "barrier" regions. Matching the wave functions and their derivatives at one interface determines two of the unknown coefficients. At the next interface, a similar procedure determines two more coefficients, but this still leaves two unknown coefficients, and on this would go *ad infinitum*. Bloch's theorem allows the second matching process to terminate the procedure, since now the two coefficients are written in terms of the original two, and we are left with four homogeneous equations with four unknowns. Because the determinant of the coefficients of these four equations must be zero for there to be a solution, one can derive the expression

$$\cos(Ka)=\cos(k_1b)\cosh[\kappa_2(a-b)]+\frac{\kappa_2^2-k_1^2}{2k_1\kappa_2}\sin(k_1b)\sinh[\kappa_2(a-b)], \tag{24}$$

where $k_1=\sqrt{2m_0E/\hbar^2}$ and $\kappa_2=\sqrt{2m_0(V_0-E)/\hbar^2}$. Equation (24) is thus an implicit equation for $E(K)$. In practice, one first selects a value of E; the absolute value of the right-hand-side of Eq. (24) is evaluated and is either greater or less than unity; if it is greater then there is no solution, but if it is less then taking the inverse cosine of this quantity gives the value of Ka for which this energy is the solution. Plots will be shown later when comparisons are made with the numerical results.

C. Matrix method for the Kronig-Penney model

It should be clear from Eq. (22) why we altered the original matrix method to use periodic boundary conditions—we simply replace Eq. (8) with Eq. (22). How does this alter the procedure discussed in subsection (III B). Quite simply, the periodicity condition (10) is modified to the Bloch condition:

$$ka=2\pi n \quad\rightarrow\quad ka=2\pi n+Ka, \tag{25}$$

where as before, $k^2=2m_0E/\hbar^2$. Hence, the basis function energies become

$$E_n^{(0)}=\frac{\hbar^2\pi^2}{2m_0a^2}\left(2n+\frac{Ka}{\pi}\right)^2=E_1^{(0)}\left(2n+\frac{Ka}{\pi}\right)^2. \tag{26}$$

Crucially, Eq. (26) modifies only the diagonal elements of the Hamiltonian. The off-diagonal elements are unaffected because the basis states (12) are modified according to

$$\phi_n^{(0)}(x)\rightarrow\frac{1}{\sqrt{a}}\exp\left[i\,\frac{2\pi n+Ka}{a}\,x\right]=e^{iKx}\phi_n^{(0)}(x). \tag{27}$$

But this means that $\phi_n^*(x)\rightarrow e^{-iKx}\phi_n^*(x)$. Thus, the extra exponentials arising from the Bloch condition cancel one another in the matrix elements H_{nm}^V and so the off-diagonal elements remain purely potential-dependent.

To locate the energy bands, we pass different values of Ka in the range $(-\pi,\,\pi)$ to matrices suitably modified by Eq. (26). The remaining matrix elements are determined as before.

As a first example, consider a unit cell consisting of a square well (Kronig-Penney model) of width b centered between two barriers of height V_0, each of width $(a-b)/2$. This is just a shifted version of Eq. (23); an example is shown in Fig. 3. Then, with $\rho \equiv b/a$ and $v_0 \equiv V_0/E_1^{(0)}$, we have the matrix

$$h_{nm} = \delta_{nm}\left[\left(2n+\frac{Ka}{\pi}\right)^2 + v_0(1-\rho)\right] + (1-\delta_{nm})v_0\frac{(-1)^{m-n+1}}{\pi}\frac{\sin[\pi(m-n)\rho]}{m-n}. \quad (28)$$

We repeatedly diagonalize matrices of this form for various values of $Ka \in (-\pi, \pi)$ to form the band solutions.

Some results for this model are shown in Fig. 4. When there are no barriers ($v_0 = V_0/E_1^{(0)} = 0$) we see the folded parabolas corresponding to plane-wave solutions. As we turn on the periodic potential (e.g., with $v_0 = 10$) we see band gaps emerge, with larger gaps in the lower-energy bands, and more curvature (i.e., band width) in the upper bands. Note that band gaps also form well above the potential barriers. Analytical solutions found by solving Eq. (24) are also shown in Fig. 4 and are in complete agreement. We have thus succeeded in demonstrating that this numerical method works for periodic arrays. The familiar result of energy bands separated by gaps with no states, owing to the limited overlap of neighboring wells, is now apparent from both a (familiar) analytical and a (less familiar) numerical point of view.

D. General potential shapes

We now have freedom to study periodic arrays of potentials with any shape, simply by performing many matrix diagonalizations (corresponding to different values of Ka) for the wave function in one unit cell. Figure 5 shows various examples of periodic potentials that we will consider here. For these potentials, it is fairly easy to compute the matrix elements analytically, as shown in Appendix A. However, it is also easy to compute the matrix elements numerically, and this approach allows treatment of a much wider range of potentials (including those for which the potential itself has no analytical form). One interesting possibility is the so-called "pseudo-Coulomb" potential

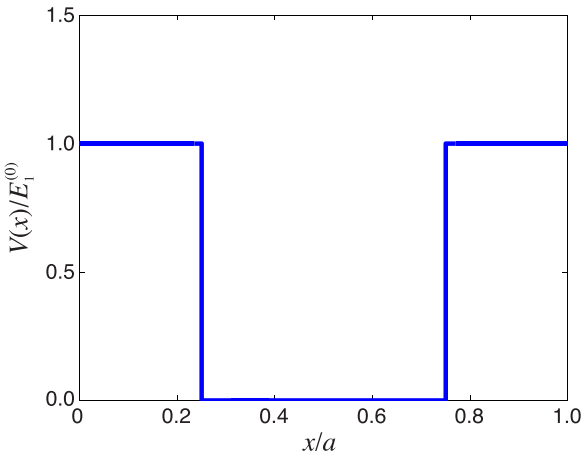

Fig. 3. Central square well with $v_0 = 1$ and $\rho = 0.5$.

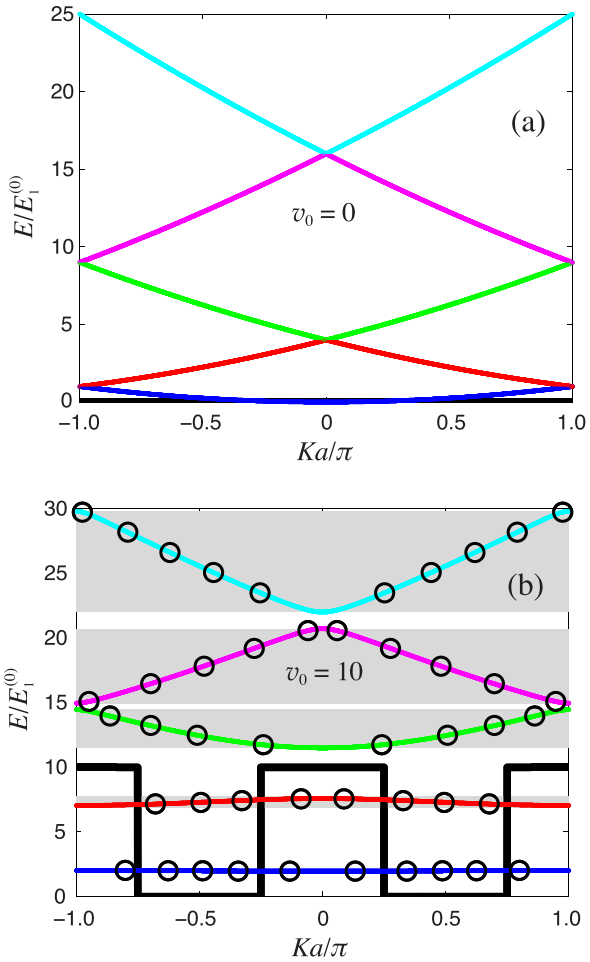

Fig. 4. Solutions to the Kronig-Penney potential with (a) no well/barrier, and (b) a repeated well/barrier sequence with barrier height $v_0 = 10$. In (b) we have also indicated with open circles some of the analytical solutions to Eq. (24). A schematic representation of the potential (as a function of x, with an arbitrary horizontal scale) is shown to indicate the boundedness of the energy bands. The matrix solutions use $n_{\max} = 60$, and we have used $\rho = b/a = 0.5$. Note that K can be varied continuously—there are no finite-size effects. We write K in terms of π/a, so the boundaries in the plot are at ± 1. For the purposes of plotting we used 1601 values of Ka/π for each band, which takes just a few seconds to run, including plotting, on an Intel 2500K processor. Readers with a background in condensed matter physics will recognize $K = \pm\pi/a$ as the boundaries of the first Brillouin zone. Note that we have lightly shaded the bands of energies where states exist. The shading is not visible behind the lowest band in the figure, because it hardly disperses.

$$v(x) = \frac{V(x)}{E_1^{(0)}} = \frac{-A}{\sqrt{(x-a/2)^2 + b^2}}, \quad (29)$$

where A is a positive number representing the strength and b is a small numerical factor introduced to prevent singularities (the true Coulomb potential is recovered as $b \to 0$), or, alternatively, the inverted pseudo-Coulomb potential with A negative.

E. Comparing band structures

Results for the band structures corresponding to the potential shapes in Fig. 5 are shown in Figs. 6–10. Sample code to produce such figures in MATLAB is provided in Appendix B, specifically for the repeating harmonic oscillator potential. We chose parameters such that in all cases three bands

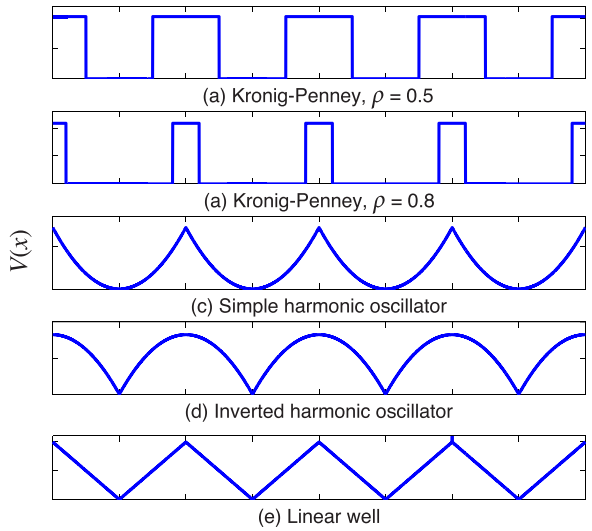

Fig. 5. Schematic representations of the potentials used for comparing energy band structures.

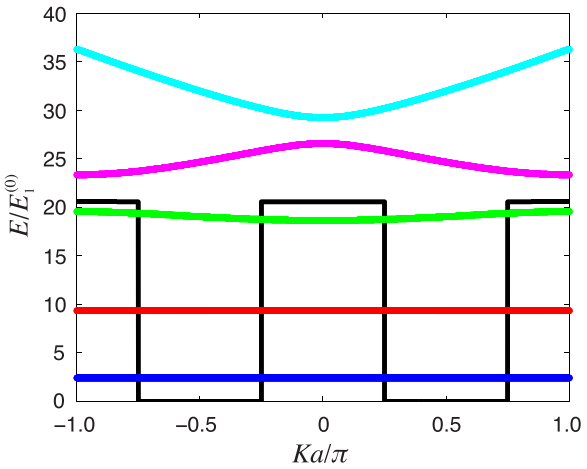

Fig. 6. Energy band diagram for the Kronig-Penney potential with $\rho = 0.5$ and $v_0 = 20.5607$ [shown here schematically and also in Fig. 5(a)]. Note the presence of energy gaps for the high-energy bands. These gaps persist with diminishing size as the energy increases.

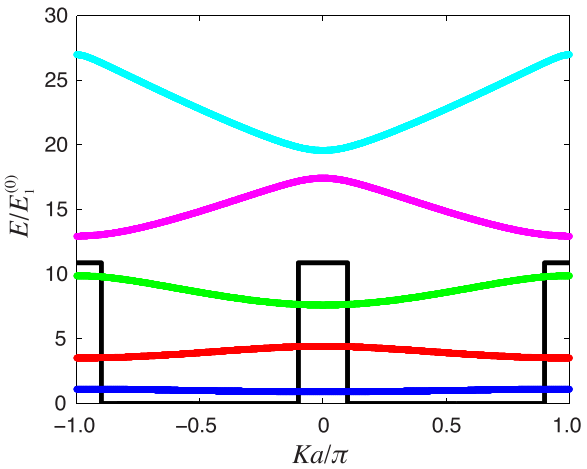

Fig. 7. Energy band diagram for the Kronig-Penney potential with $\rho = 0.8$ and $v_0 = 10.8775$ [shown here schematically and also in Fig. 5(b)].

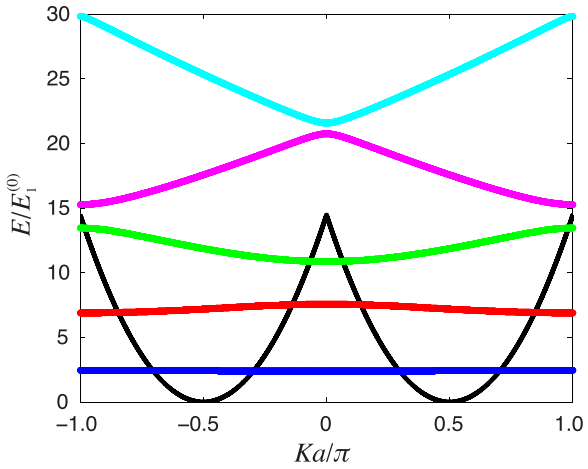

Fig. 8. Energy band diagram for the simple harmonic oscillator potential with $\gamma = \hbar\omega/E_1^{(0)} = 4.84105$ [shown here schematically and also in Fig. 5(c)]. Note the small energy gap separating the two highest energy bands (compared with that arising from the Kronig-Penney potential shown in the previous two figures). This gap is even smaller for the inverted harmonic oscillator potential (Fig. 9) and the linear well potential (Fig. 10).

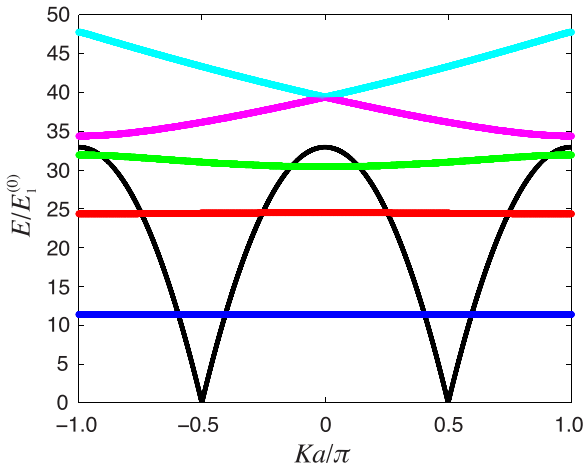

Fig. 9. Energy band diagram for the inverted harmonic oscillator potential with $\gamma = \hbar\omega/E_1^{(0)} = 7.30845$ [shown here schematically and also in Fig. 5(d)]. Note the very small gap between the two highest energy bands, and also the non-parabolic dispersion for these two bands.

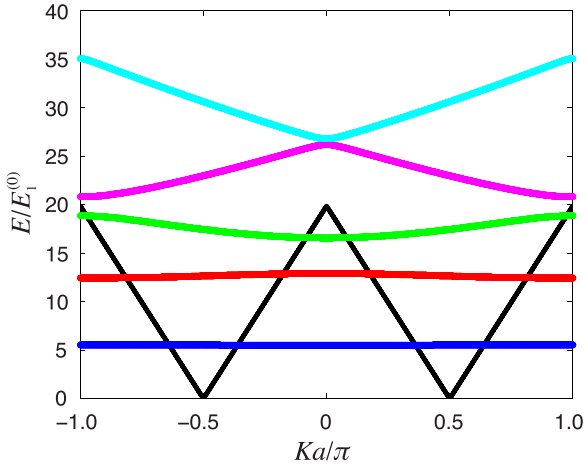

Fig. 10. Energy band diagram for the linear well potential with $A = 19.8705$ [shown here schematically and also in Fig. 5(e)]. The comments in the previous two figure captions apply here as well.

with energies less than the maximum barrier height would form, and in which the third band would have an energy difference between the highest level (at $Ka = \pm\pi$) and the maximum barrier potential $V_{\max}$ of $\Delta E = E_1^{(0)}$.

As mentioned earlier, bands with gaps form at energies above the barrier maxima as well. However, the character of these bands is strongly dependent on the type of periodic potential used. In particular, for the last three potentials shown in Fig. 5 the gap can be quite small (not even discernible, for example, on the scale of Fig. 9). Moreover, for these last three potentials, the minima and maxima of these higher energy bands can be distinctly non-parabolic, and in fact exhibit V-shaped (or inverted V-shaped) dispersions close to the minima (or maxima).

For each of these five potentials, we then focused on the third band (the one closest to but lower than $V_{\max}$) and normalized the bands by setting the highest band level to $E = 0$ in each case, as shown in Fig. 11. The band width varies considerably as shown; this can be adjusted by varying the barrier heights and widths, as is explicitly shown in the case of the Kronig-Penney model (first two potentials of Fig. 5); in the case of the other potentials, we could include an additional barrier or well "plateau."

One property of importance is the ratio of the electron and hole effective masses. These are defined through the correspondence of the band dispersion with the free-electron-like parabolic behavior at the minima and maxima of the bands, respectively. It is well known in the semiconductor community that the hole effective mass at the top of the valence band can differ considerably from the electron effective mass at the bottom of the (next) conduction band. However, many of the models utilized by researchers in the field of strongly correlated electron systems have electron-hole symmetry; this means that the electron and hole effective masses *in the same band* are identical. These effective masses are defined by

$$\frac{1}{m_e^*} \equiv \frac{1}{\hbar^2}\frac{d^2E(K)}{dK^2}\bigg|_{K_{\min}} \quad \text{and} \quad \frac{1}{m_h^*} \equiv \frac{1}{\hbar^2}\frac{d^2E(K)}{dK^2}\bigg|_{K_{\max}}. \tag{30}$$

Derivations of these equations can be found in solid state physics textbooks, but a heuristic argument can be made by

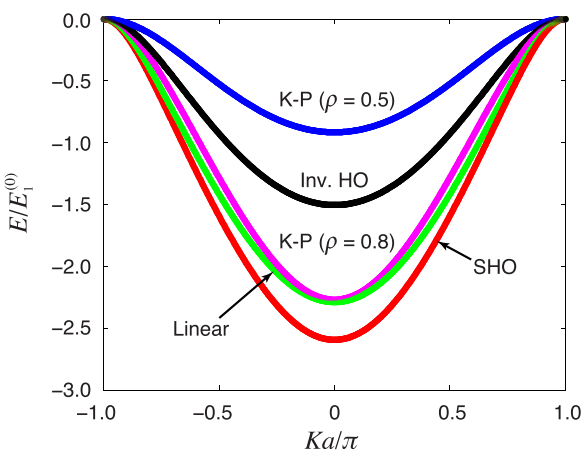

Fig. 11. The third energy band for the five potentials shown in Fig. 5, with the topmost energy set equal to zero. Note the variation in bandwidth, but, more importantly, the difference in curvatures, as tabulated in Table I.

Table I. The dimensionless second derivatives at the minimum (maximum) of the third energy bands from Fig. 11, which are inversely proportional to the electron and hole effective masses. The third column gives the ratio $e''_e/e''_h \equiv m_h^*/m_e^*$.

Potential	e''_e	e''_h	e''_e/e''_h
K-P ($\rho = 0.5$)	13.83	−25.35	−0.55
K-P ($\rho = 0.8$)	39.09	−70.61	−0.55
Simple HO	37.84	−121.80	−0.31
Inverted HO	19.83	−55.96	−0.35
Linear	31.63	−102.23	−0.31

comparing to the free-electron case where the kinetic energy is given by $E = \hbar^2K^2/(2m_0)$. Taking two derivatives of the kinetic energy with respect to the momentum gives the reciprocal of the mass, and so in our case we take derivatives using the *crystal momentum* $\hbar K$ for the same effect.

We evaluate the second derivative in Eq. (30) using a five-point fit[12] and tabulate the ratio m_h^*/m_e^* of the two effective masses for each potential shape in Table I, where we also tabulate the dimensionless second derivatives $e_i'' \equiv (\pi^2/a^2)\, d^2e_i(K)/dK^2$, with $i = e$ (electron) or h (hole). That is, these second derivatives are computed directly from the data points in Fig. 11 at the points $Ka/\pi = 0$ and 1. The ratio depends on the details of the potential used; the two Kronig-Penney models yield essentially the same ratio, and the magnitude of this ratio can decrease considerably with other potential shapes. From the data in Table I, first note that the ratio has a magnitude that is less than unity. This is because holes have effectively a weaker barrier through which to tunnel compared with electrons. Consider the third band in any of Figs. 6–10 and imagine two cases: the band is nearly empty of electrons (many holes) or the band is nearly full of electrons (few holes). For the nearly empty case, electrons will occupy the lowest-energy states near $K = 0$ and so, relative to their energy level, will see a higher potential step than in the case where the band is nearly filled with electrons near $K = \pm\pi/a$.

The decrease of the ratio m_h^*/m_e^* below unity is most pronounced when either the linear or simple harmonic oscillator potential is used. The reason is that these potentials have cusp-like barriers, so that the barrier width is also reduced for holes compared to electrons; therefore, the holes should have more mobility (lower effective mass) compared with electrons, over and above the advantage already present due to the difference in effective barrier height. For Figs. 8–10 and looking at the third band once again, we see that the potentials "look" wider for those states around $K = 0$ than for those states near $K = \pm\pi/a$.

This asymmetry between electrons and holes may be important in a new class of superconducting models, where dynamic interactions are taken into account.[13,14]

V. SUMMARY

We hope that this paper will serve as a bridge from the classroom to the research desk for both undergraduate and graduate students in the area of electronic structure calculations. The "classroom" or "textbook" example for electronic band structure has always been the Kronig-Penney model. The enlightening feature in the model has been the recasting of the problem of an extended (i.e., Bloch) state in terms of the problem in one unit cell, using Bloch's theorem. The part

that is more intimidating for students is the extension beyond simple square wells to more realistic potentials; this is what this paper has tried to address.

Simple procedures to obtain numerical solutions for any potential that supports bound states were illustrated in Ref. 4. This methodology was extended to periodic boundary conditions for the purpose of this paper, because the next step—implementing the Bloch condition—is then essentially trivial. Students can then tackle their own favorite potential, such as the "pseudo-Coulomb" potential referred to in Eq. (29). We have given a number of examples already in this paper and mentioned one particular property, the asymmetry between electron and hole masses, that can have important consequences for semiconductors and possibly superconductors. In general, the more realistic potentials tend to make the barrier effectively narrower for holes than for electrons, with the consequence that hole masses are generally lower than electron masses. We also note that more realistic potentials can give rise to higher energy bands with non-parabolic shapes.

ACKNOWLEDGMENTS

This work was supported in part by the Natural Sciences and Engineering Research Council of Canada (NSERC), by the Alberta iCiNano program, and by a University of Alberta Teaching and Learning Enhancement Fund (TLEF) grant.

APPENDIX A: ANALYTICAL MATRIX ELEMENTS

For the harmonic oscillator [Fig. 5(c)], beginning with Eq. (18) we can cast the integral into the dimensionless form (recall that $\gamma \equiv \hbar\omega/E_1^{(0)}$)

$$h_{nm}^V \equiv \frac{H_{nm}^V}{E_1^{(0)}} = \left(\frac{\pi\gamma}{2}\right)^2 I_{nm}, \tag{A1}$$

where

$$I_{nm} = (-1)^{m-n}\int_{-1/2}^{1/2} u^2 e^{i2\pi(m-n)u}\,du. \tag{A2}$$

This integral is elementary and the required dimensionless matrix elements with the Bloch modification are

$$h_{nm} = \delta_{nm}\left[\left(2n+\frac{Ka}{\pi}\right)^2 + \frac{\pi^2\gamma^2}{48}\right] + (1-\delta_{nm})\left[\frac{\gamma^2}{8}\frac{1}{(m-n)^2}\right]. \tag{A3}$$

For the inverted harmonic oscillator potential [Fig. 5(d)], we use

$$V(x) = \begin{cases} -\frac{1}{2}m_0\omega^2\left[x^2 - \frac{a^2}{4}\right] & 0 < x < \frac{a}{2}, \\ -\frac{1}{2}m_0\omega^2\left[(x-a)^2 - \frac{a^2}{4}\right] & \frac{a}{2} < x < a. \end{cases} \tag{A4}$$

This system has matrix elements

$$h_{nm} = \delta_{nm}\left[\left(2n+\frac{Ka}{\pi}\right)^2 + \frac{\pi^2\gamma^2}{24}\right] - (1-\delta_{nm})\left[\frac{\gamma^2}{8}\frac{(-1)^{m-n}}{(m-n)^2}\right]. \tag{A5}$$

Note the difference between Eqs. (A5) and (A3) in both the off-diagonal elements (change of sign) and the diagonal elements (factor of 2 in the potential term).

A third example is the linear well [Fig. 5(e)], with potential defined by

$$V(x) = \begin{cases} 2A\left(\frac{1}{2} - \frac{x}{a}\right) & 0 < x < \frac{a}{2}, \\ 2A\left(\frac{x}{a} - \frac{1}{2}\right) & \frac{a}{2} < x < a. \end{cases} \tag{A6}$$

This system has matrix elements

$$h_{nm} = \delta_{nm}\left[\left(2n+\frac{Ka}{\pi}\right)^2 + \frac{A}{2}\right] - (1-\delta_{nm})\frac{A}{\pi^2(m-n)^2}\left[1-(-1)^{m-n}\right]. \tag{A7}$$

APPENDIX B: SAMPLE CODE

Here, we present some MATLAB code that will populate a matrix with the harmonic oscillator unit cell matrix elements (the `harmosccell` function), which is then used to generate the energy bands and plot them (the `bandcalc` function). To reproduce the results of Fig. 8, one can run the command:

```
≫ bandcalc (60, 4.84105, 800)
```

```
function h = harmosccell (N, g)
%HARMOSCCELL Simple harmonic oscillator unit cell matrix elements
% N x N matrix
% g is the strength of the SHO in units of \hbar \omega/E_1^(0)
h = zeros (1,N+1);
%OEIS A001057 = 0, 1, -1, 2, -2,…
a = @(n) (1 - (2*n+1)*(-1)^n)/4;
% Precompute a(n) values
an = zeros (1, N+1);
for i = 1:N+1
  an(i) = a(i-1);
end
% Compute diagonal elements
n = 1:N+1;
h = 4*an(n).*an(n) + (pi*pi*g*g)/48;
% - (4*an(n)*Ka/pi) + (Ka*Ka)/(pi*pi))
h = diag(h);
% Compute off-diagonal upper triangular elements
% m = an(n+1:end), n = an(n)
for n = 1:N
  h(n,n+1:end) = (1/8)*g*g*((-1).^(an(n+1:
  end) -an(n))./…
  ((an(n+1:end)-(an(n))).^2);
end
```

```
% Fill the LL with the conjugate transpose of
UR
h=h+triu(h, 1)';
end

function [E, Ka] =bandcalc(N, g, iter)
%BANDCALC Generates energy bands for repeat-
ing harmonic oscillator
% N x N matrix
% g is the strength of the SHO in units of
\hbar \omega/E_1^(0)
% Number of points per band=2*iter+1 (sym-
metric around 0)
E=zeros(N+1,2*iter+1);
Ka=0:(pi/(iter)):pi; % Generate values of
Ka from 0 to pi
Ka=horzcat(-fliplr(Ka(2:length(Ka))), Ka);
% Mirror to -pi to 0
%OEIS A001057=0, 1, -1, 2, -2,...
a=@(n)(1-(2*n+1)*(-1)^n)/4;
h=harmosccell (N, g); % Solve matrix ele-
ments once
% Precompute a(n) values
an=zeros (1, N+1);
for i=1:N+1
  an(i)=a(i-1);
end
for i=1:iter+1
  hbloch=h;
  % Modify main diagonal with Bloch
  condition
  for n=1:N+1
    hbloch(n,n)=hbloch(n,n)-(4*an(n)*Ka(i)/
    pi)+(Ka(i)*Ka(i))/(pi*pi);
  end
  % Diagonalize matrix and store energe
  results
  [c, Ebloch]=eig (hbloch);
  Ebloch=diag(Ebloch);
  E(:,i)=sort (real (Ebloch));
  E(:,2*iter-i+2)=E(:,i);
end
% Plotting
for i=1:2*iter+1
  plot (Ka(i)/pi, E(1,i),'b.','MarkerSize',
  13);
  plot (Ka(i)/pi, E(2,i),'r.','MarkerSize',
  13);
  plot (Ka(i)/pi, E(3,i),'g.','MarkerSize',
  13);
  plot (Ka(i)/pi, E(4,i),'m.','MarkerSize', 13);
  plot (Ka(i)/pi, E(5,i),'c.','MarkerSize',
  13);
  hold on;
end
xlabel('Ka/\pi','FontSize', 16);
ylabel('E/E_1{(0)}','FontSize', 16);
end
```

[a]Electronic mail: rpavelic@ualberta.ca
[b]Electronic mail:fm3@ualberta.ca

[1]R. de L. Kronig and W. G. Penney, "Quantum mechanics of electrons in crystal lattices," Proc. R. Soc. London Ser A **130**, 499–513 (1931).
[2]F. Bloch, "Über die Quantenmechanik der Elektronen in Kristallgittern," Z. Phys. **52**, 555–600 (1929), in German. Remarkably, Bloch has 12 papers that are more cited than this one. See also F. Bloch, "Memories of electrons in crystals," Proc. R. Soc. London Ser A **371**, 24–27 (1980), where he provides some context for this theorem.
[3]Almost any introductory condensed matter textbook will introduce some basic notions about electronic band structure. A particularly lucid account that tries to take you from the basic Kronig-Penney model to more sophisticated calculations is N. W. Ashcroft and N. D. Mermin, *Solid State Physics* (Saunders, Philadelphia, 1976), chaps. 8–11.
[4]F. Marsiglio, "The harmonic oscillator in quantum mechanics: A third way," Am. J. Phys. **77**, 253–258 (2009).
[5]V. Jelic and F. Marsiglio, "The double-well potential in quantum mechanics: A simple, numerically exact formulation," Eur. J. Phys. **33**, 1651–1666 (2012).
[6]I. D. Johnston and D. Segal, "Electrons in a crystal lattice: A simple computer model," Am. J. Phys. **60**, 600–607 (1992).
[7]See Ref. 4. Note that this article has a typographical error in Eq. (15), which has been corrected here in Eq. (17).
[8]Mathworks, MATLAB function eig, <http://www.mathworks.com/help/matlab/ref/eig.html>.
[9]G. Lindfield and J. Penny, *Numerical Methods: Using MATLAB*, 3rd ed. (Academic Press, Waltham, MA, 2012), pp. 135–138.
[10]E. Gkioulekas, "Algorithms with Matlab," <faculty.utpa.edu/gkioulekase/codes/matlab_lalg.pdf>, pp. 12–16.
[11]In either case, for the harmonic oscillator potential, or any potential that is even in x, we could of course increase the efficiency by a factor of 2 by leaving out the even-integer basis functions for the infinite square well case (since they are zero) and using only the sum of the positive and negative coefficients for the periodic boundary condition case. In a more general case neither of these efficiencies is possible.
[12]T. Pang, *An Introduction to Computational Physics*, 2nd ed. (Cambridge U.P., Cambridge, 2006), p. 51.
[13]J. E. Hirsch, "Dynamic hubbard model," Phys. Rev. Lett. **87**, 206402-1–4 (2001).
[14]G. H. Bach, J. E. Hirsch, and F. Marsiglio, "Two-site dynamical mean field theory for the dynamic Hubbard model," Phys. Rev. B **82**, 155122-1–15 (2010) and references therein.